A Methodology for Probabilistic Fault Displacement Hazard Analysis (PFDHA)

Robert R. Youngs, M.EERI, Walter J. Arabasz, M.EERI, R. Ernest Anderson, Alan R. Ramelli, Jon P. Ake, M.EERI, David B. Slemmons, M.EERI, James P. McCalpin, Diane I. Doser, Christopher J. Fridrich, Frank H. Swan III, M.EERI, Albert M. Rogers, M.EERI, James C. Yount, Laurence W. Anderson, Kenneth D. Smith, Ronald L. Bruhn, Peter L.K. Knuepfer, Robert B. Smith, Craig M. dePolo, M.EERI, Dennis W. O'Leary, Kevin J. Coppersmith, M.EERI, Silvio K. Pezzopane, David P. Schwartz, M.EERI, John W. Whitney, Susan S. Olig, M.EERI, and Gabriel R. Toro, M.EERI

Robert R Youngs

Geomatrix Consultants, Inc.

2101 Webster St, 12th Floor

Oakland, CA 94612

phone: 510-663-4231

fax: 510-663-4141

email: byoungs@geomatrix.com

Submission date for review copies: November 6, 2000

Submission date for camera-ready copy:

A Methodology for Probabilistic Fault Displacement Hazard Analysis (PFDHA)

Robert R. Youngs, M.EERI, Walter J. Arabasz, M.EERI, R. Ernest Anderson, Alan R. Ramelli, Jon P. Ake, M.EERI, David B. Slemmons, M.EERI, James P. McCalpin, Diane I. Doser, Christopher J. Fridrich, Frank H. Swan III, M.EERI, Albert M. Rogers, M.EERI, James C. Yount, Laurence W. Anderson, Kenneth D. Smith, Ronald L. Bruhn, Peter L.K. Knuepfer, Robert B. Smith, Craig M. dePolo, M.EERI, Dennis W. O'Leary, Kevin J. Coppersmith, M.EERI, Silvio K. Pezzopane, David P. Schwartz, M.EERI, John W. Whitney, Susan S. Olig, M.EERI, and Gabriel R. Toro, M.EERI

We present a methodology for conducting a site-specific probabilistic analysis of fault displacement hazard. Two approaches are outlined. The first relates the occurrence of fault displacement at or near the ground surface to the occurrence of earthquakes in the same manner as is done in a standard probabilistic seismic hazard analysis (PSHA) for ground shaking. The methodology for this approach is taken directly from PSHA methodology with the ground motion attenuation function replaced by a fault displacement attenuation function. In the second approach, the rate of displacement events and the distribution for fault displacement are derived directly from the characteristics of the faults or geologic features at the site of interest. The methodology for probabilistic fault displacement hazard analysis (PFDHA) was developed for a normal faulting environment and the probability distributions we present may have general application in similar tectonic regions. In addition, the general methodology is applicable to any region and we indicate the type of data needed to apply the methodology elsewhere.

(RRY) Geomatrix Consultants, 2101 Webster St., 12th Fl, Oakland, CA 94612, byoungs@geomatrix.com; (WJA) Univ. of Utah, 135 S 1460 E, Rm 705, Salt Lake City, UT 84112; (REA) USGS, Denver Federal Center, MS 966, PO Box 25007, Denver, CO 80255; (ARR) Nevada Bureau of Mines and Geology, Univ. of Nevada, Reno, NV 89557, (JPA) USBR, Denver Federal Center, MC-3611, PO Box 25007, Denver, CO 80225; (DBS) 2905 Autumn Haze Ln, Las Vegas, NV, 89117; (JPM) GEO-HAZ, PO Box 837, Crestone, CO 81131; (DID) Dept. of Geological Sciences, Univ. of Texas, El Paso, TX 79968; (CJF) USGS, Denver Federal Center, MS 913, PO Box 25046, Denver, CO 80225; (FHS) 240 Laidley St., San Francisco, CA 94131; (AMR) GeoRisk Associates, 17214 Rimrock Dr, Golden, CO 80401; (JCY) USGS, Mackay School of Mines MS 176, Univ. of Nevada, Reno, NV, 89557; (LWA) USBR, Denver Federal Center, D-8330, PO Box 25007, Denver, CO 80225; (KDS) Seismological Lab. MS 168, Mackay School of Mines MS 176, Univ. of Nevada, Reno, NV, 89557; (RLB) Dept of Geology and Geophysics, Univ. of Utah, Salt Lake City, UT, 84112; (PLKK) Dept. of Geological Sciences, State Univ. of New York, Binghamton, NY 13902; (RBS) Dept of Geology and Geophysics, Univ. of Utah, Salt Lake City, UT, 84112; (CMdP) Nevada Bureau of Mines and Geology, Univ. of Nevada, Reno, NV 89557; (DWO) USGS, Denver Federal Center, MS 425, PO Box 25046, Denver, CO 80255; (KJC) Coppersmith Consulting, 2121 N. California Blvd, Suite 290, Walnut Creek, CA 94596; (SKP) USGS, Denver Federal Center, MS 425, PO Box 25046, Denver, CO 80255; (DPS) USGS; 345 Middlefield Rd, MS 977, Menlo Park, CA 94025; (JWW) USGS, Denver Federal Center, MS 425, PO Box 25046, Denver, CO 80255; (SSO) URS, Inc. 500 12th St., Suite 200, Oakland, CA 94607; (GRT) Risk Engineering, Inc., 4155 Darley Ave, Suite A, Boulder, CO 80303

INTRODUCTION

Probabilistic seismic hazard analysis (PSHA) has been used for evaluation of ground shaking hazards and establishing seismic design parameters since its development in the late 1960s and early 1970s (Cornell 1968, 1971). The effects of ground shaking, notably soil liquefaction and landslides, have also been analyzed probabilistically in several studies (e.g., Power et al. 1991). In contrast, probabilistic methods have not been applied to any great extent in the evaluation of fault rupture hazard. In part, this may be because the primary method for mitigating fault displacement hazard is avoidance, an option not available for ground shaking hazard. For facilities that cannot use avoidance, notably pipelines, deterministic hazard evaluations are typically used because the hazard mitigation design solutions are not greatly sensitive to the amount of displacement. For other facilities, such as roads, the design solution is often to accept the risk of displacement and plan for rapid post-earthquake repair.

There are situations where a facility may not have the option of complete avoidance, and where the design solutions are sensitive to the amount of displacement. One such facility is the potential high-level nuclear waste repository that is proposed for Yucca Mountain, Nevada. A number of block bounding and minor faults and a complex pattern of fracturing have been identified within the proposed repository footprint and across access routes. Because of the large area require for the repository, it is not possible to avoid all faults. Design of pre-closure waste handling and emplacement facilities, as well as evaluation of post-closure performance requires an assessment of the hazard posed by potential displacements on these faults and fractures.

The design process for the repository is based on a probabilistic treatment of hazards, such as ground shaking, to establish design levels that have an acceptably low probability of being exceeded. The methodology for probabilistic assessment of ground shaking hazard is well established in the design community and is described in detail in several of documents (e.g., NRC 1988, SSHAC 1997). In contrast, the methodology for probabilistic assessment of fault displacement hazard was not as well established. Thus, a significant effort went into the development of a probabilistic fault displacement hazard analysis (PFDHA) methodology for the project. The complete study is documented in CRWMS M&O (1998). An overview of the complete PSHA analysis and a summary of the results are presented in Stepp et al. (2001). This paper describes the formulation of a PFDHA methodology and the various probabilistic models that can be used to assess the hazard. The paper summarizes work performed by the many authors in their roles as experts for the Yucca Mountain project and in subsequent applications of the methodology to other sites.

Two basic approaches are presented for PFDHA. The first, called the *earthquake approach*, is derived from the PSHA formulation for ground shaking hazard and relates the occurrence of displacement on a feature at a site at or near the ground surface explicitly to the occurrence of earthquakes (fault slip at depth) in the site region. The feature in question may be a fault, a minor shear, a fracture, or unbroken ground. The second, called the *displacement approach*, utilizes the characteristics of fault displacement observed at the site of interest to quantify the hazard without invoking a specific mechanism for their cause. In this paper we describe the two approaches for PFDHA developed for the Yucca Mountain project focusing on aspects that have a wider application to assessing fault displacement hazards at other sites. We also list in the Appendix various probability distributions based on regional or global data sets that are illustrative of the types of distributions needed to perform a PFDHA and may be applicable to assess hazards in regions characterized by normal

faulting. Application of this methodology to the assessment of fault displacement hazard should include a formal treatment of uncertainties using the approaches that have become standard for ground motion PSHA studies.

EARTHQUAKE APPROACH FOR PFDHA

The earthquake-approach formulation that is used for PFDHA is directly taken from that for ground motion PSHA. PSHA is usually expressed in terms of the annual rate of earthquakes in which a ground motion parameter, Z, (e.g., peak ground acceleration, peak response spectral acceleration) exceeds a specified level, z at site k. This rate of exceedance, $n_k(z)$, is computed by the expression (Cornell 1968, 1971):

$$n_k(z) = \sum_n a_n(m^0) \int_{m^0}^{m_n^u} f_n(m) \left[\int_0^\infty f_{kn}(r|m) \cdot P(Z > z|m,r) \cdot \mathrm{d}r \right] \cdot \mathrm{d}m \qquad (1)$$

where $a_n(m^0)$ is the rate of all earthquakes on source n above a minimum magnitude of engineering significance, m^0; $f_n(m)$ is the probability density of earthquake size between m^0 and a maximum earthquake that source n can produce, m_n^u; $f_{kn}(r \mid m)$ is the conditional probability density function for distance from site k to an earthquake of magnitude m occurring on source n; and $P(Z>z \mid m,r)$ is the conditional probability that, given an earthquake of magnitude m at distance r from site k, the peak ground motion will exceed level z. [In practice, the density functions $f_n(m)$ and $f_{kn}(r \mid m)$ are replaced by discrete mass functions $P_n(M=m_i)$ and $P_{kn}(R=r_j \mid m_i)$, and the integrals of Equation 1 are replaced by summations.] The term $P(Z>z \mid m,r)$ relates the occurrence of ground motion at the site to the occurrence of an earthquake through a ground motion attenuation model.

Using the formulation of Equation 1, an earthquake-based approach to assessing the rate at which the displacement, D, on a feature exceeds a specified amount, d, during a single event can be expressed as:

$$n_k(d) = \sum_n a_n(m^0) \int_{m^0}^{m^u} f_n(m) \left[\int_0^\infty f_{kn}(r|m) \cdot P_{kn}^*(D > d|m,r) \cdot \mathrm{d}r \right] \cdot \mathrm{d}m \qquad (2)$$

where $P_{kn}^*(D>d \mid m,r)$ is an "attenuation function" for fault displacement at or near the ground surface. We use P^* because the displacement attenuation function differs from the usual ground motion attenuation function in that it contains two terms, specifically:

$$P_{kn}^*(D > d|m,r) = P_{kn}(\mathrm{Slip}|m,r) \cdot P_{kn}(D > d|m,r,\mathrm{Slip}) \qquad (3)$$

The first term of Equation 3, $P_{kn}(\mathrm{Slip} \mid m,r)$, is the conditional probability that some amount of displacement occurs at k as a result of an earthquake (fault slip at depth) on source n of magnitude m with rupture at a distance of r from the site. In PSHA it is assumed that each earthquake produces some level of ground shaking at site k [$P_{kn}(\mathrm{shaking} \mid m,r) = 1$], though it may be very weak. However, not every earthquake results in fault offset at every site. The trace of the principal fault rupture may be discontinuous and distributed ruptures occur at discrete locations.

The second term of **(3)** defines the conditional distribution of the amount of fault displacement given that slip occurs. This probability is computed using a continuous distribution with parameters that are functions of m and perhaps r in the same manner that ground motion attenuation relationships typically define lognormal distributions for Z as

functions of m and r. The conditional probability $P_{kn}(D>d \mid m,r,\text{Slip})$ is given subscripts because it may depend on more than just m and r, unlike the standard ground motion attenuation relationship. For example, the displacement may depend on the relative location of the site along the length of the fault rupture.

The parallelism between PSHA and the earthquake approach to PFDHA is illustrated schematically on Figures 1 and 2. Figure 1 shows the steps in PSHA. First, potential seismic sources are identified, represented in this case by a fault. The rate of occurrence of earthquakes of various sizes on the fault is characterized by a recurrence relationship that defines $a_n(m^0)$ and $f_n(m)$ in **(1)**. The conditional distribution $f_{kn}(r \mid m)$ is computed by randomly locating a rupture appropriate for magnitude m on the fault (illustrated by the heavy line) and computing the distance from the rupture to the site. The conditional probability of exceeding ground motion level z, $P(Z>z \mid m,r)$, is obtained using a ground motion attenuation relationship that specifies the conditional probability distribution for Z (peak acceleration in this example) as a continuous function of m and r. These are combined to produce a ground motion hazard curve that relates the ground motion level z to the rate that it is exceeded.

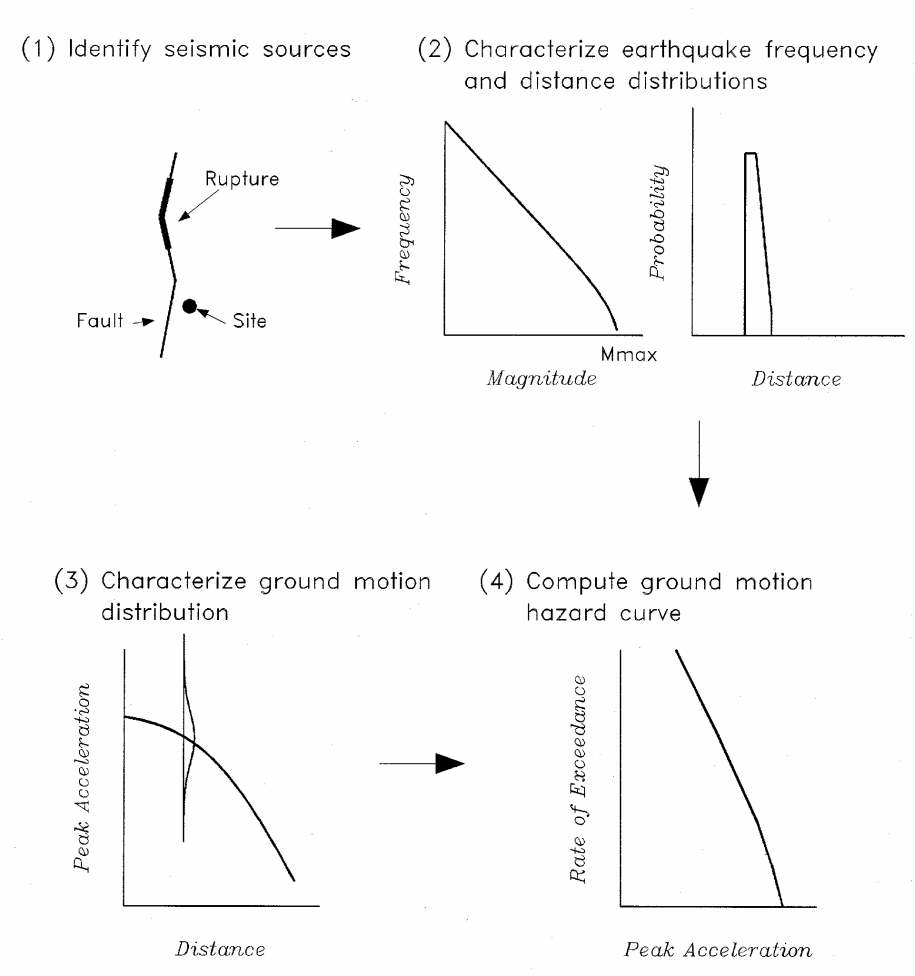

Figure 1. Schematic diagram illustrating the components of PSHA for ground shaking.

Figure 2 shows the equivalent steps in the earthquake approach to PFDHA. Source identification and characterization of the rate and size distribution of earthquakes are identical to those steps in PSHA. The distance distribution is computed in the same manner as for PSHA. However, additional information on the geometry of the ruptures may be

retained for defining the displacement, as will be described subsequently. The conditional probability of exceeding displacement d, $P_{kn}^{*}(D>d \mid m,r)$, is computed using a displacement attenuation relationship that differs from that for ground motion in that there is a finite probability that no slip will occur [equal to the conditional probability $1\text{-}P_{kn}(\text{Slip} \mid m,r)$]. The probability distributions are again combined to develop a displacement hazard curve that relates the displacement d at point k in a single event to the rate that it is exceeded. The characteristics of displacement hazard curves are described in the discussion section of this paper.

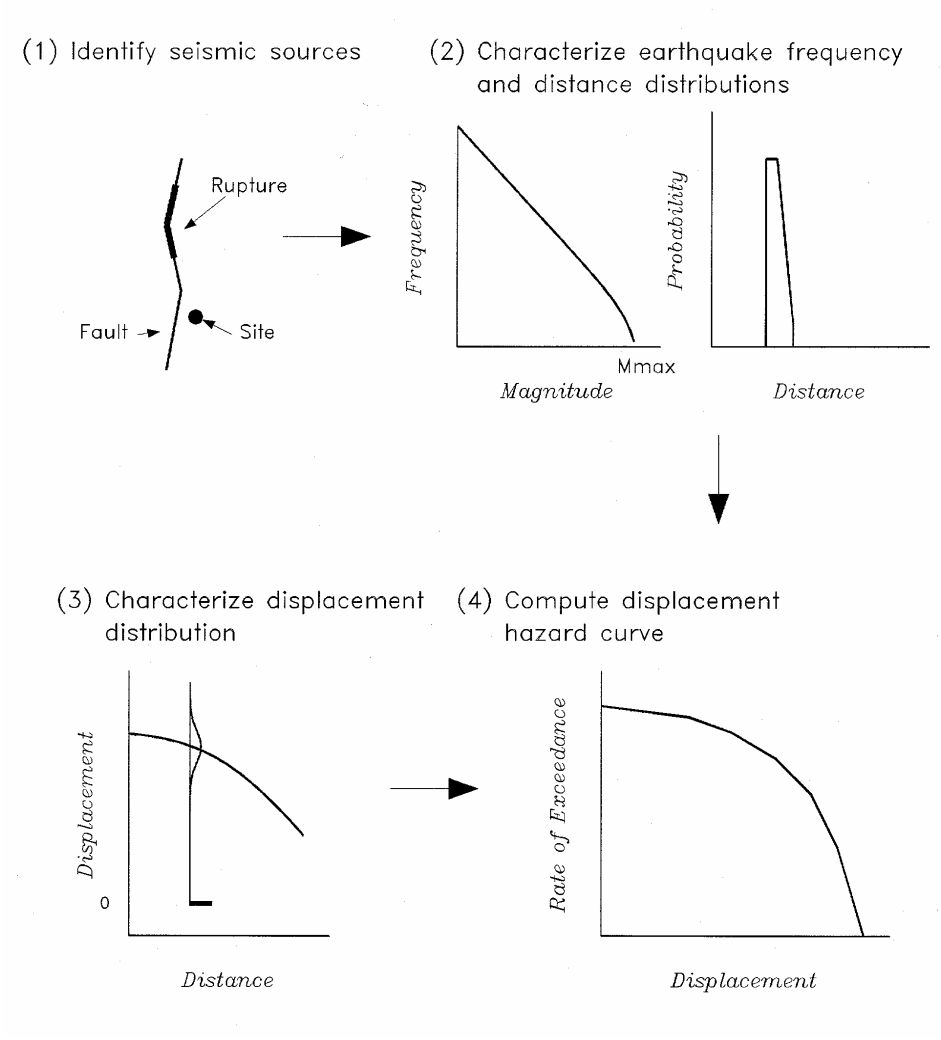

Figure 2. Schematic diagram illustrating the components of the earthquake approach to PFDHA.

At this point we introduce the distinction between two types of fault displacement: *principal faulting* and *distributed faulting*. These are illustrated on Figure 3, which shows the characterization of principal and distributed faulting for several Basin and Range earthquakes. Principal faulting is slip along the main plane (or planes) of crustal weakness responsible for the release of seismic energy during the earthquake. Where the principal fault rupture extends to the surface, it may be represented by displacement along a single narrow trace or over a zone that may range from a few to many meters wide. The faults of concern are those that may produce earthquakes (i.e., are directly related to the primary source of energy release). Principal faulting is the type of fault displacement hazard that has typically been evaluated in the past.

Distributed faulting is defined as displacement that occurs on other faults, shears, or fractures in the vicinity of the principal rupture in response to the principal faulting. It is expected that distributed faulting will be discontinuous in nature and occurs over a zone that may extend outward several tens of meters to many kilometers from the principal rupture. A fault that can produce principal rupture may also undergo distributed faulting in response to principal rupture on other faults. These distinctions are important because different models and data sets are used to assess the terms of Equation 3 depending on the type of faulting being evaluated, principal or distributed.

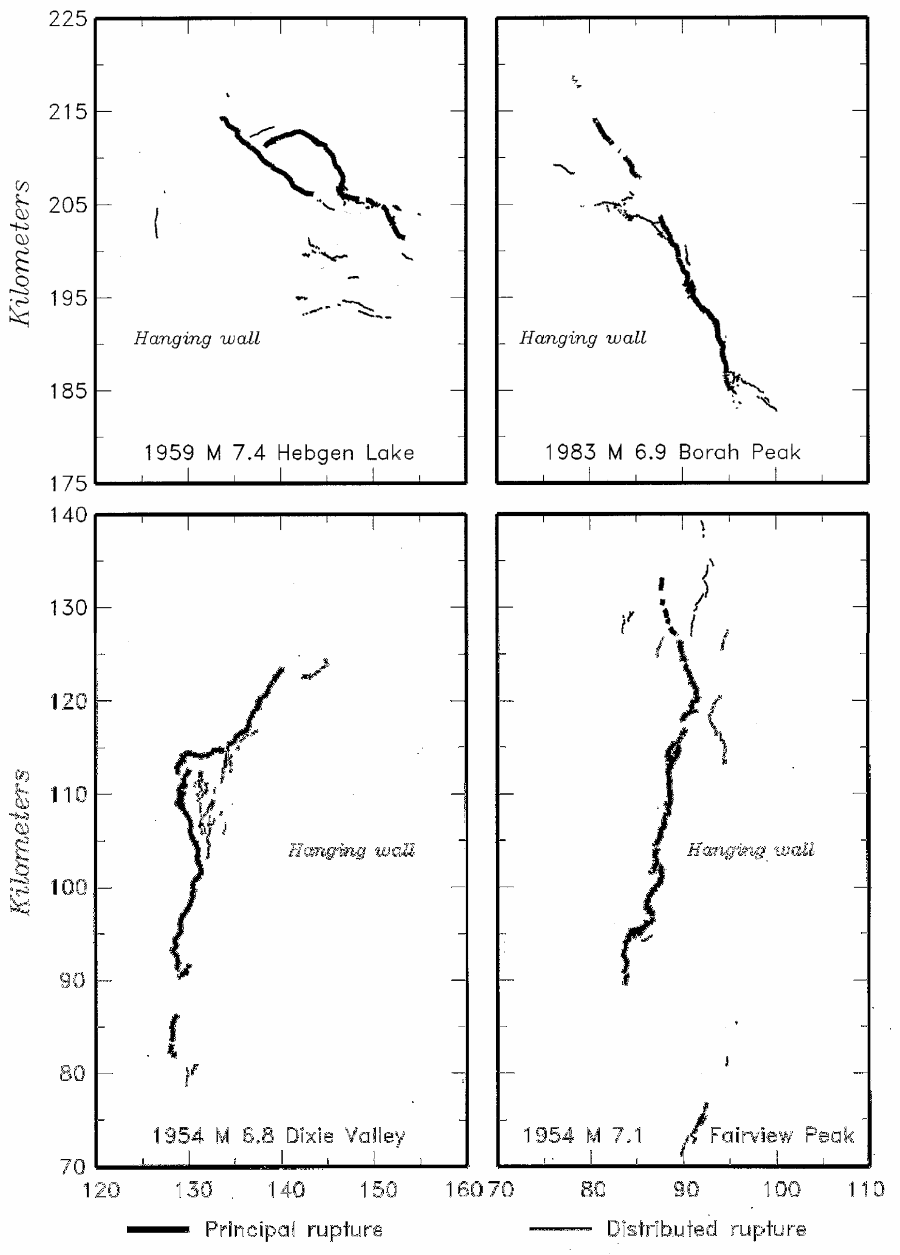

Figure 3. Example mapped displacement patterns showing principal and distributed faulting (data from Pezzopane and Dawson, 1996).

MODELS FOR PRINCIPAL FAULTING

Conditional Probability of Slip

The term $P_{kn}(\text{Slip} \mid m,r)$ for principal faulting expresses the conditional probability that the rupture on the fault causing the earthquake reaches the surface (or near the surface for assessments of underground facilities) at location k on that fault. This probability can be computed using either simulation or empirical models.

Where seismic sources are represented as planar faults in a standard PSHA, the conditional probability distribution for the distance from the earthquake rupture to the site is typically computed numerically. For an earthquake of magnitude m_i the length and down-dip width are computed from empirical relationships. The rupture area is then randomly placed on the fault plane according to specified distributions and the distance to the site computed for each location to construct $P_{kn}(R=r_j \mid m_i)$. Typically, it is assumed that the rupture location is uniformly distributed along the length of the fault. The down-dip location of the rupture is based on the observed hypocenter depth distribution for the region and the hypocenter is assumed to be located within the rupture area according to a specified distribution, such as uniformly distributed in the lower half of the rupture. For the case where site k is located on the fault trace, then $P_{kn}(\text{Slip} \mid m,r)$ in Equation 3 is equal to $P_{kn}(R=0 \mid m_i)$.

As an alternative, an empirical approach can be used to compute the conditional probability that the rupture will reach the surface. Wells and Coppersmith (1993), dePolo (1994), and Pezzopane and Dawson (1996) present data sets that define the rate at which earthquakes of various magnitudes rupture the surface. Wells and Coppersmith (1993) used a *logistic regression* model to evaluate the conditional probability of surface rupture. The logistic regression model (e.g., Hosmer and Lemeshow 1989) is a commonly used model for assessing the outcome of a dichotomous variable – given the occurrence of an earthquake, surface rupture either occurs or does not occur. The probability of a positive outcome (the occurrence of principal surface rupture given the occurrence of the earthquake) is given by the expression (Wells and Coppersmith 1993):

$$P(\text{principal surface rupture}) = \frac{e^{f(x)}}{1+e^{f(x)}} \qquad \text{with} \quad f(x) = a + bm \tag{4}$$

where m is earthquake magnitude, and parameters a and b are estimated from the data. Figure 4 presents the results of fitting Equation 4 to the various data sets presented by Pezzopane and Dawson (1996) for surface rupture as a function of earthquake magnitude for Basin and Range normal faulting earthquakes. Also shown for comparison is the relationship obtained by Wells and Coppersmith (1993) for a worldwide data set of all slip types. The parameters of these models are listed in the Appendix. These conditional distributions combined with a conditional distribution for the location of the rupture along the length of the fault provides an assessment of $P_{kn}(\text{Slip} \mid m,r)$ for principal rupture.

Conditional Probability of Exceedance

The conditional probability that the displacement will exceed a specified value d given slip occurs from a magnitude m earthquake at a distance r from the site, $P_{kn}(D>d \mid m,r,\text{Slip})$, can be assessed using models built on empirical data, much as ground motion attenuation

relationships are constructed. The conditional probability $P_{kn}(D>d \mid m,r,\text{Slip})$ represents the probability that at a specific point *k* on a rupture the fault displacement exceeds *d*. Figure 5 shows the variation in amount of surface displacement along the principal rupture for historical Basin and Range normal faulting events compiled by Wheeler (1989). The displacements are normalized by the maximum displacement, *MD*, measured for each rupture. These data were used to define a distribution for the ratio *D/MD*. The distribution for *D/MD* is expressed as a function of the location of point *j* along the rupture, denoted by the ratio *x/L*, where *x* is the distance from one end of the rupture to point *j* and *L* is the length of rupture. The distribution was constructed by assuming that *D/MD* is limited to the range of 0 to 1 and $f(D/MD \mid x/L)$ is symmetric about $x/L = 0.5$. Although the rupture patterns shown on Figure 5 are not symmetric about $x/L = 0.5$, one does not know before hand whether one is at the end of the rupture with the larger or smaller displacements. Combining the data symmetrically about $x/L = 0.5$ results in a larger variability in the model to reflect this uncertainty.

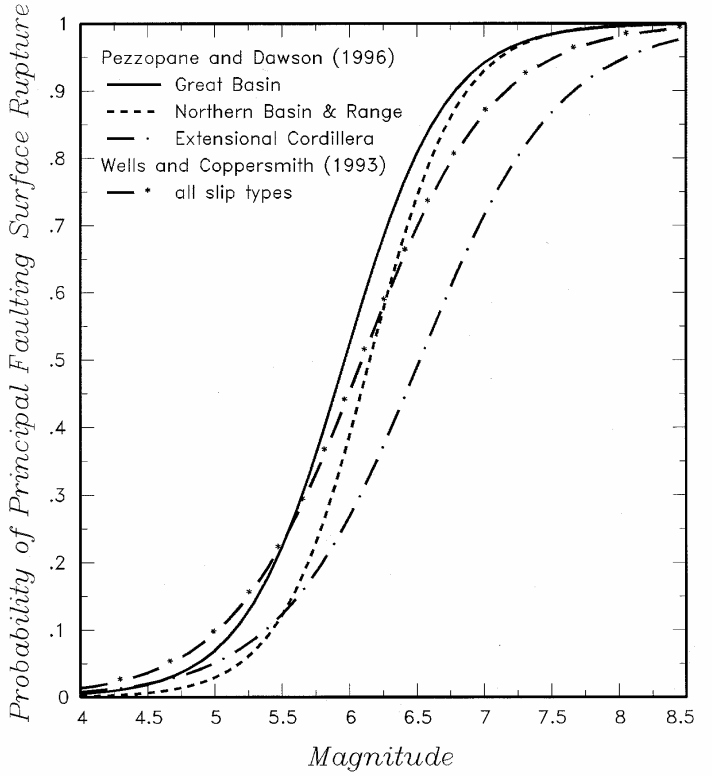

Figure 4. Empirical models for conditional probability of surface rupture for principal faulting obtained from Equation 4 with parameters determined from the indicated data sets. (The parameters are listed in the Appendix.)

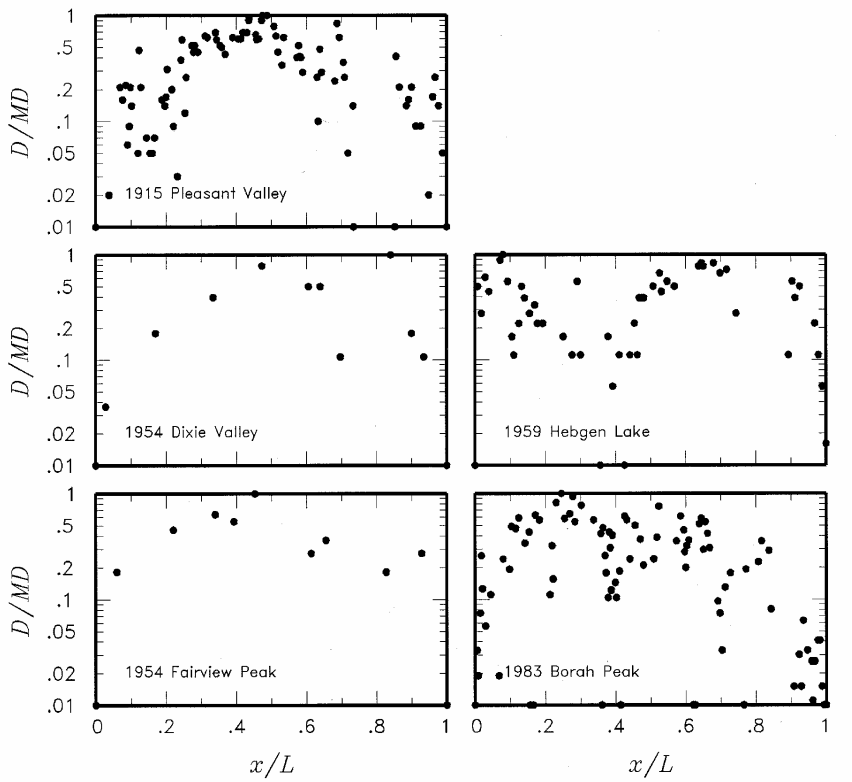

Figure 5. Principal faulting displacement distributions for the five historical ruptures presented in Wheeler (1989).

A very flexible distribution for modeling variables that have a fixed range is the beta distribution. When the variable y is limited to the range $0 \le y \le 1$, the beta distribution has the form:

$$F(y) = \frac{\Gamma(a+b)}{\Gamma(a)\Gamma(b)} \int_0^y z^{a-1}(1-z)^{b-1} dz \qquad (5)$$

where $\Gamma(\ )$ is the gamma function and $F(y)$ is the cumulative probability that variable Y is less than or equal to a specific value y. The data shown on Figure 5 were smoothed by eye by J. McCalpin to form three curves representing the minimum, median, and maximum values of the ratio *D/MD* as a function of *x/L*. These curves are shown on the left of Figure 6. Setting y = *D/MD*, and assuming that the minimum curve represents the 5th percentile and the maximum curve represents the 95th percentile, beta distribution parameters were defined as functions of *x/L* (see the Appendix). Shown on the right of Figure 6 are examples of the resulting cumulative distribution functions (CDF's) for *D/MD*.

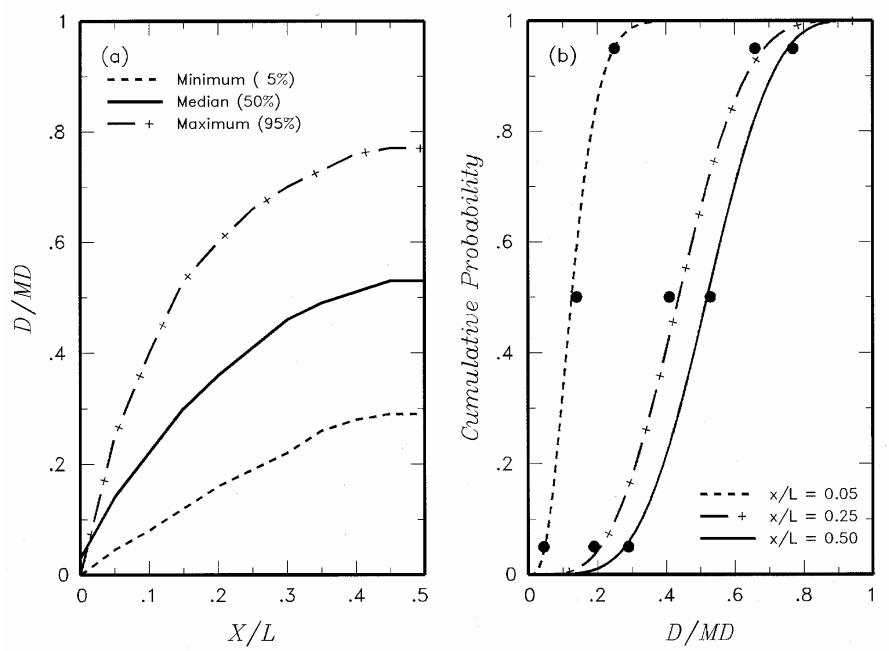

Figure 6. Distribution for the ratio *D/MD* based on the data in Wheeler (1989). (a) Curves defining the range in *D/MD* smoothed by eye by J. McCalpin for the Yucca Mountain PSHA using the data shown on Figure 5. (b) Cumulative distributions for beta distributions fit to the curves in (a). The dots indicate the values from (a).

An evaluation of the maximum displacement during an individual earthquake is needed to complete the assessment of $P_{kn}(D>d \mid m,r,\text{Slip})$. Empirical distributions for *MD* as a function of earthquake magnitude have been published recently by Wells and Coppersmith (1994). The conditional probability of exceedance, $P_{kn}(D>d \mid m,r,\text{Slip})$, can be obtained by convolving Equation 5 with the lognormal distribution for *MD*. Note that the computation of $P_{kn}(D>d \mid m,r,\text{Slip})$ requires assessment of the ratio *x/L* for each rupture location. As a result, the conditional probability of slip $P_{kn}(\text{Slip} \mid m,r)$ and the conditional probability of exceedance $P_{kn}(D>d \mid m,r,\text{Slip})$ must be computed jointly.

As an alternative, the displacement along the length of the rupture can be normalized by the average displacement that occurred, *AD*, and the distribution for *D/AD* fit with an appropriate probability model. $P_{kn}(D>d \mid m,r,\text{Slip})$ is then computed by convolving the distribution for *D/AD* with an empirical distribution for *AD* as a function of earthquake magnitude (e.g., Wells and Coppersmith 1994).

More extensive data sets of mapped displacement distributions for historical ruptures has been compiled and analyzed by McCalpin and Slemmons (1998) and Hemphill-Haley and Weldon (1999). Figure 7 shows the data from McCalpin and Slemmons (1998) displayed in terms of *D/MD* and *D/AD*. The data for *D/MD* were fit with a beta distribution model with parameters that are functions of *x/L* (see the Appendix). The resulting percentiles of the distribution are shown on the upper panel of Figure 7. The ratio *D/AD* is limited to positive values and may be skewed to the right. A flexible distribution of this type is the gamma distribution, which has the cumulative form:

$$F(y) = \frac{1}{\Gamma(a)} \int_0^{y/b} e^{-t} t^{a-1} dt \qquad (6)$$

where $\Gamma(\ )$ is again the gamma function. Setting y equal to D/AD and making the parameters a and b functions of x/L, we obtain the percentiles shown on the lower panel of Figure 7. The relationships for parameters a and b obtained by fitting the data shown on Figure 7 are listed in the Appendix.

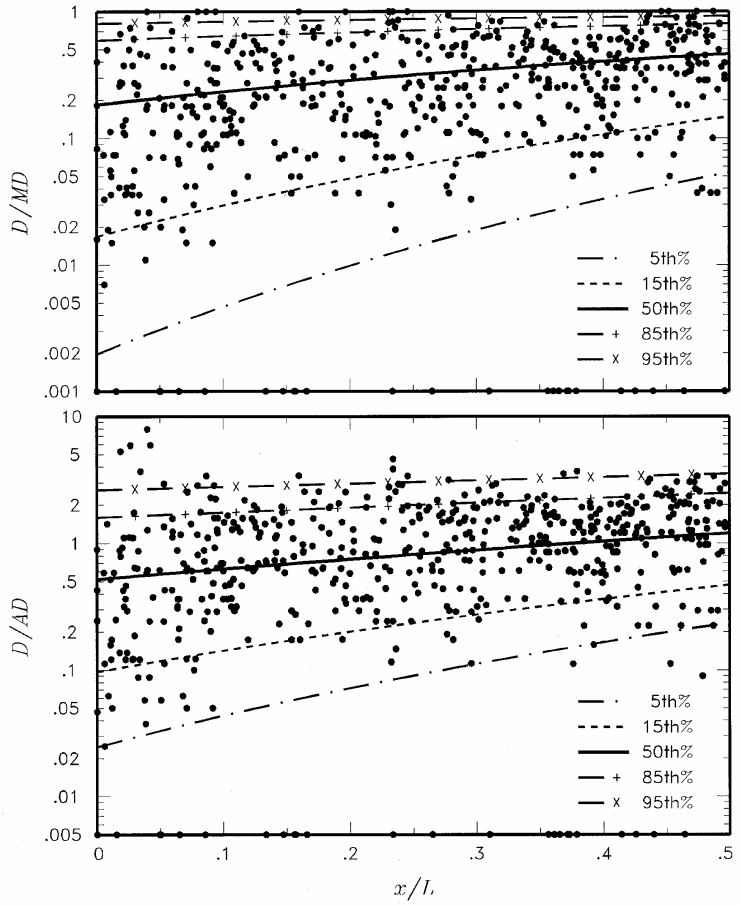

Figure 7. Combined data sets for *D/MD* and *D/AD* from McCalpin and Slemmons (1998) for 11 normal faulting earthquakes. The curves show the percentiles of the beta (*D/MD*) and gamma (*D/AD*) distributions fit to the data.

Figure 8 shows the conditional probability of exceedance, $P_{kn}(D>d \mid m,r,\text{Slip})$, for three values of *x/L* and for magnitude 6 and 7 earthquakes. The complementary-cumulative distributions were obtained by convolving the distributions for *D/MD* or *D/AD* shown on Figures 6 and 7 with lognormal distributions for *MD* or *AD* from Wells and Coppersmith (1994) for normal faulting earthquakes. The variability between the different conditional probabilities of exceedance curves shown on Figure 8 results from the broader distribution shown on Figure 7 compared to that on Figure 6, differences between the magnitude scaling in the Wells and Coppersmith (1994) relationships for *AD* and *MD*, and differences in the shape of the gamma and beta distributions. In addition, the relationships shown on Figure 6a were constrained to approach zero displacement at the ends of the rupture while those shown on Figure 7a were not constrained, allowing for the potential of large displacements very near the end of the fault rupture. These differences are analogous to variability in the conditional probability of exceeding ground shaking levels computed using alternative ground motion attenuation models in a ground shaking PSHA and emphasize the importance of considering alternative approaches and models in performing a PFDHA.

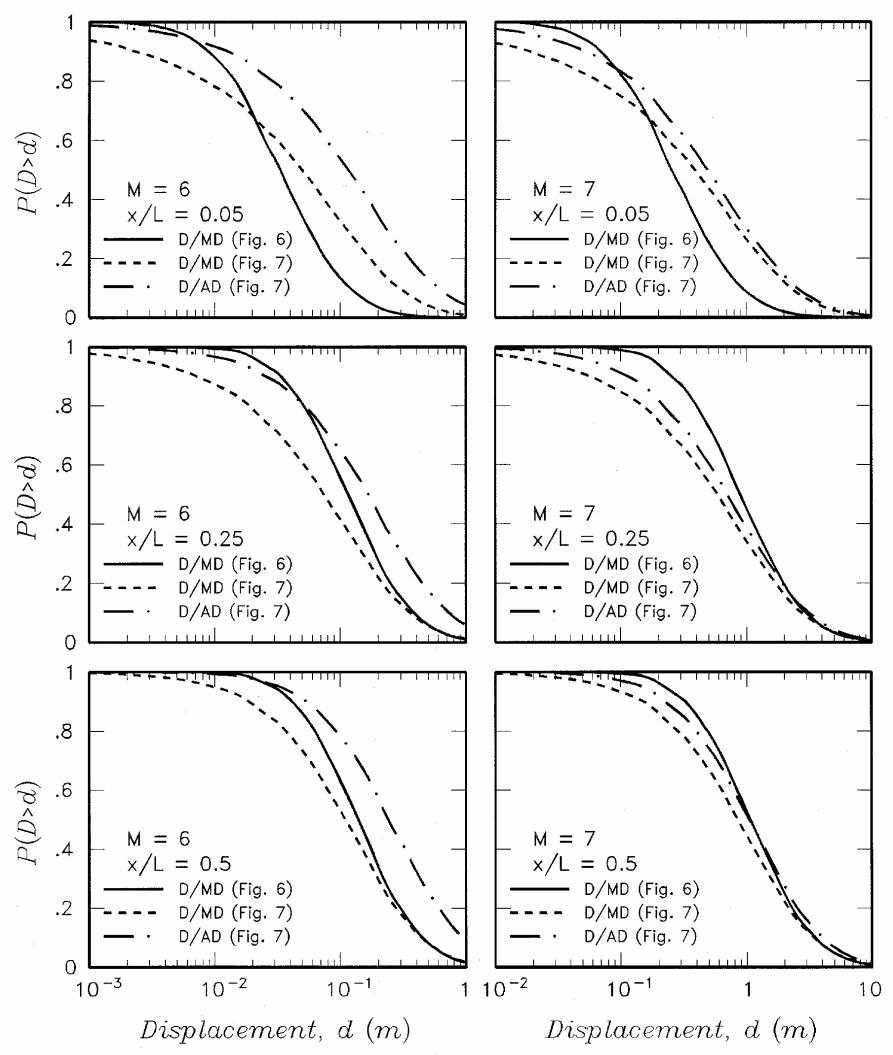

Figure 8. Conditional distributions for the probability of exceeding various values of principal faulting displacement. $P_{kn}(D>d \mid m,r,\text{Slip})$ is computed by convolving distributions for *D/MD* and *D/AD* shown on Figures 6 and 7 with lognormal distributions for *MD* and *AD* for normal faulting earthquakes from Wells and Coppersmith (1994). Plots are shown for **M** 6 and 7 and for x/L = 0.05, 0.25 and 0.5.

MODELS FOR DISTRIBUTED FAULTING, EARTHQUAKE APPROACH

Conditional Probability of Slip

The term $P_{kn}(\text{Slip} \mid m,r)$ for distributed faulting expresses the conditional probability that surface (or near-surface) displacement occurs on a feature at location *k* due to an earthquake occurring on some other source. Distributed slip on both minor and major faults adjacent to the principal faulting rupture is presumed to be causally linked to the primary rupture, but the causal mechanism usually is not sufficiently understood, and there may be multiple mechanisms at work. We have taken an empirical approach to define this probability function, using data from historical ruptures.

Pezzopane and Dawson (1996) present a set of maps of historical ruptures that have occurred in the extensional cordillera of the western United States on which they indicate the

location of distributed (secondary) ruptures around the principal (primary) fault rupture. Examples of these ruptures are shown on Figure 3. Several patterns are observable from these data. The amount of distributed rupture increases with the size of the earthquake and decreases with distance from the principal rupture. In addition, the density of distributed ruptures is greater in the hanging wall than in the footwall of the principal (normal fault) ruptures.

The data presented by Pezzopane and Dawson (1996) were digitized by constructing a raster scan of each map using a 0.5-km × 0.5-km pixel size. The number of pixels containing distributed faulting divided by the total number of pixels within the faulting area gives a measure of rate of occurrence of distributed rupture for each earthquake. Figure 9 presents the data obtained from analyzing the rupture maps of Pezzopane and Dawson (1996). The data represent 13 earthquakes ranging in magnitude from **M** 5.5 to **M** 7.4. The data are plotted in terms of rate of distributed faulting as a function of distance from the principal rupture and location on the hanging wall or footwall. The rate is computed as the number of pixels with distributed faulting divided by the total number of pixels within 0.5-km distance increments from the principal rupture. Each point represents the rate of distributed rupture at a specific distance for a single earthquake, with the earthquake magnitude indicated by the symbol type. The rows of data at the bottom of each plot represent data from an individual earthquake where there were zero observations of distributed faulting at a given distance from the principal rupture.

The data shown on Figure 9 also represent the outcome of a dichotomous variable — distributed rupture either occurs or does not occur at each point (represented in this case by a 0.25 km^2 pixel). The logistic regression model was used to compute the conditional probability of distributed rupturing occurring at a point. The data were fit with a functional form that incorporates the observed trends of decreasing frequency with increasing distance, increased density with increasing magnitude, and lower frequency and faster decrease in frequency with increasing distance in the footwall than in the hanging wall:

$$P(\text{distributed surface rupture}) = \frac{e^{f(x)}}{1+e^{f(x)}}$$
$$\text{with } f(x) = C_1 + (C_2 + C_3 m + C_4 h)\cdot \ln(r + C_5) \tag{7}$$

where m is again earthquake magnitude, r is the distance to the principal rupture (km), and h is an indicator variable taking the value of 1 for the hanging wall side of the rupture and 0 for the footwall side of the rupture. The dashed curves shown on Figure 9 are the result of fitting Equation 7 to the data shown on the figure. These curves represent a balance between the nonzero frequency data points scattered throughout the plots and the zero frequency data represented by the rows of points at the bottom of the plots.

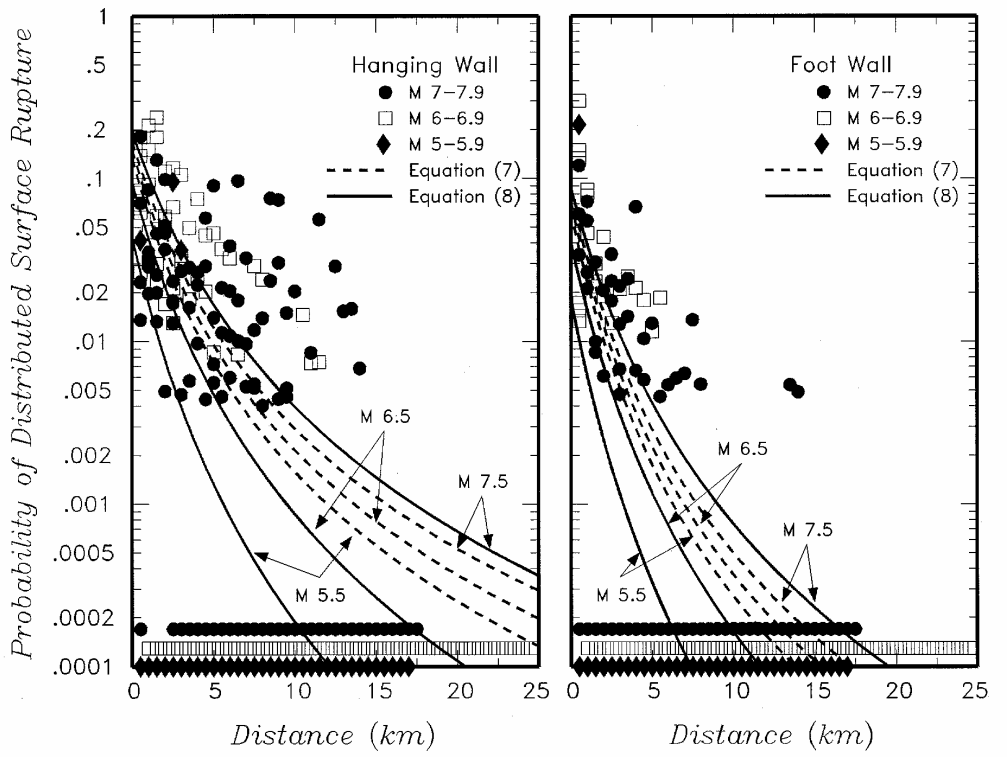

Figure 9. Conditional probability of slip, $P_{kn}(\text{Slip} \mid m,r)$, for distributed faulting. Symbols show the rate of occurrence of distributed faulting for individual earthquakes (data from Pezzopane and Dawson, 1996). The curves show $P_{kn}(\text{Slip} \mid m,r)$ for specific magnitudes using Equations 7 and 8.

The maps compiled by Pezzopane and Dawson (1996) show a large variability in the density of distributed faulting between earthquakes of similar magnitude, indicating that there may be other important factors not accounted for by Equation 7. Improving the fit of a predictive model usually requires adding additional terms using other explanatory variables and/or cross products of the variables. However, it is not clear what other variables to add in this case. An alternative approach is to represent the unknown variables by a random variate (e.g., Brillinger and Preisler, 1983). Equation 7 is modified to the form:

$$f(x) = C_1 + (C_2 + C_3 m_i + C_4 h) \cdot \ln(r + C_5) + t\ z_i \qquad (8)$$

where z_i is a normal variate with 0 mean and unit variance representing a random effect for the i^{th} event and t is the measure of variability from event to event. This model assumes that there are unknown characteristics not accounted for in Equation 7 that vary randomly from earthquake to earthquake. Brillinger and Preisler (1983) present a general approach for estimating the coefficients of Equation 8 using maximum likelihood combined with Gaussian quadrature. The resulting fit to the data is shown by the solid lines on Figure 9 for the case of $z_i = 0$ (the average behavior). Hosmer and Lemeshow (1989, page 141) define a goodness of fit statistic, $\hat{C}$, as a Pearson χ^2 statistic for a table of observed and predicted frequencies for grouped data. Use of this statistic for the data grouped by each earthquake indicates that Equation 8 results in an improved prediction of the observed frequencies of distributed faulting compared to Equation 7. The parameters of both are listed in the Appendix.

The model described above assumes that the mapping data for the historical ruptures is complete. Incomplete mapping would lead to an underestimate of the rate of distributed rupture. However, this possible deficiency is counterbalanced by the assumption in our application that

the occurrence of distributed rupture anywhere within a 0.5 km ×0.5 km square is considered to be the same as the occurrence of rupture at the point of interest. This assumption is likely to produce an overestimate of the rate of occurrence at a point (such as a building footprint with an area << 0.25 km^2). We postulate that the use of the large pixel size more than compensates for the effect of incomplete mapping.

We also investigated the influence of the angle q between the strike of the fault with the principal rupture and the strike of the individual faults with distributed rupture on the relative rate of distributed slip. The digitized maps of historical ruptures of Pezzopane and Dawson (1996) were analyzed to calculate the strike azimuths of the principal faulting trace and the individual distributed faulting traces by minimizing the squared distance from the fault trace digitization points measured normal to the strike line. The top plot of Figure 10 shows the data in terms of the frequency of ruptures in each 5° increment of q (the number of ruptures in each increment divided by the total number of ruptures). The number of digitization points for each distributed rupture trace is indicated on the figure. It is expected that the estimate of the true strike of a trace is improved as the number of digitization points is increased.

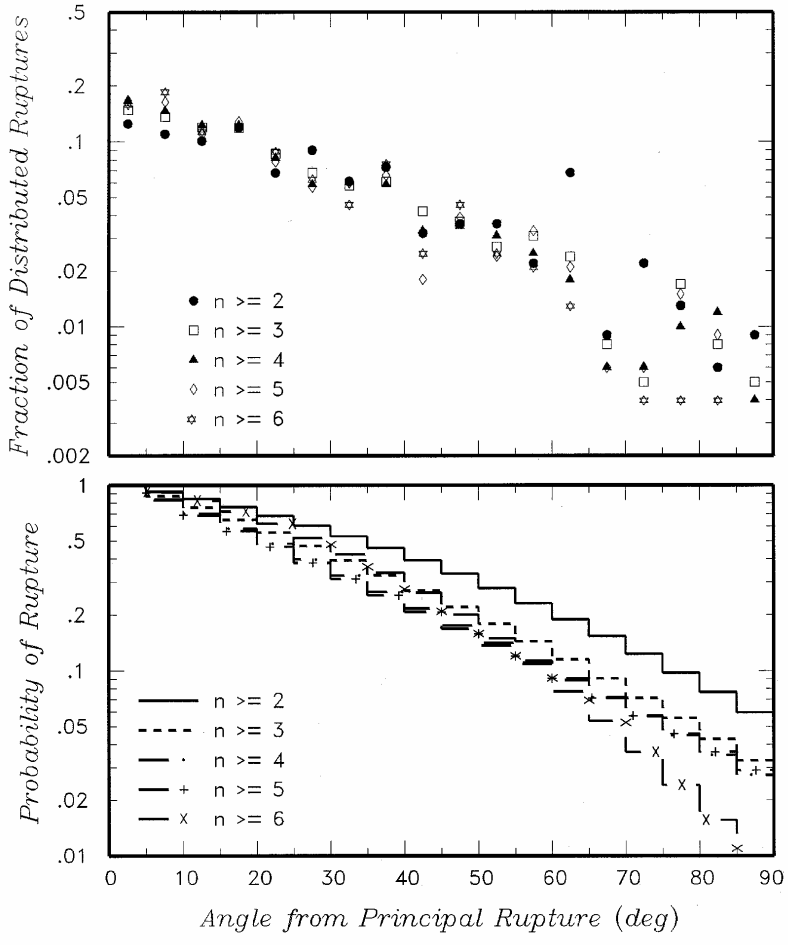

Figure 10. Effect of azimuth on frequency of distributed slip. (a) Relative frequency of distributed slip as a function of the angle, q between the strike of the distributed fault and the strike of the principal rupture. (b) Results of fitting Equation 9 to the data in (a) normalized to give a probability of 1 at $q = 0$.

The frequency data plotted at the top of Figure 10 were fit with the functional form:

$$\ln(\ frequency) = C_1 + C_2\,\mathrm{int}(q\ /\ 5) + C_3\,\mathrm{int}(q\ /\ 5)^2 \qquad (9)$$

where int( ) is the integer function [i.e., int(4/5) = 0, int(7/5) = 1]. The parameters obtained for the various data sets are listed in the Appendix. Equation 9 can be used to assess the relative probability of slip as a function of q by assuming that the probability is unity at q = 0 (i.e., setting C_1 to 0 in Equation 9**)**. The lower plot on Figure 10 shows the resulting relationships for the different data sets.

Conditional Probability of Exceedance

Unlike principal faulting, there are very limited data for the amount of slip that occurs on the secondary features that move during distributed faulting. For example, in compiling their database of maps of historical ruptures, Pezzopane and Dawson (1996) were able to find many fewer reported offsets on distributed rupture features. Previous evaluations of distributed faulting (McGuire et al. 1990, Coppersmith and Youngs 1992) were also able to find only limited data for the amount of slip that occurs in distributed faulting. Typically the principal rupture is mapped and described in much greater detail than the distributed ruptures, which are more numerous and widely dispersed, yet smaller in size, and unlikely to be preserved for older events.

Figure 11 shows the data compiled by C. dePolo for the ratio of the displacement on a distributed rupture, $D_{distributed}$, to the maximum displacement on the associated principal rupture, $MD_{principal}$, for normal faulting earthquakes. Also shown on Figure 11 are curves that are postulated to represent a high percentile of the distribution of possible displacements that may occur on a distributed rupture (in the range of the 85th to 95th percentile of the distribution for $D_{distributed}/MD_{principal}$). The curves were constructed to conform to the general trends observed in the density of distributed faulting data; that is, greater amplitude in the hanging wall and a more rapid falloff in amplitude with distance in the footwall. The equations describing these curves are listed in the Appendix. The distribution for $D_{distributed}/MD_{principal}$ can then be defined by specifying a probability distribution form and anchoring the appropriate percentile of that distribution to the curves shown on Figure 11. For example, we have found that a gamma distribution (e.g., Equation 6) with a shape parameter, a, near 2.5 adequately describes the distribution of individual displacements observed on a feature. The 95th percentile of a gamma distribution with a equal to 2.5 occurs at x/b equal to 5.535. Setting x in Equation 6 equal to $D_{distributed}/MD_{principal}$, the value of parameter b at a given distance from the principal rupture is found by dividing the value of $D_{distributed}/MD_{principal}$ shown on Figure 11 by 5.535. The conditional probability of exceedance, $P_{kn}(D>d \mid m,r,\mathrm{Slip})$, is then obtained by convolving the resulting gamma distribution for $D_{distributed}/MD_{principal}$ with a distribution for MD on the principal rupture (such as the lognormal distributions given by Wells and Coppersmith 1994) in the same manner as was done for principal faulting. If the curves shown on Figure 11 are assumed to represent the 85th percentile, then parameter b at a given distance from the principal rupture is found by dividing the value of $D_{distributed}/MD_{principal}$ shown on Figure 9 by 4.058. Other distributions could also be used, such as a log normal with a specified coefficient of variation.

An alternative approach for specifying $P_{kn}(D>d \mid m,r,\mathrm{Slip})$ utilizes solely the characteristics of the feature of interest. These methods will be described in the next section outlining the displacement approach.

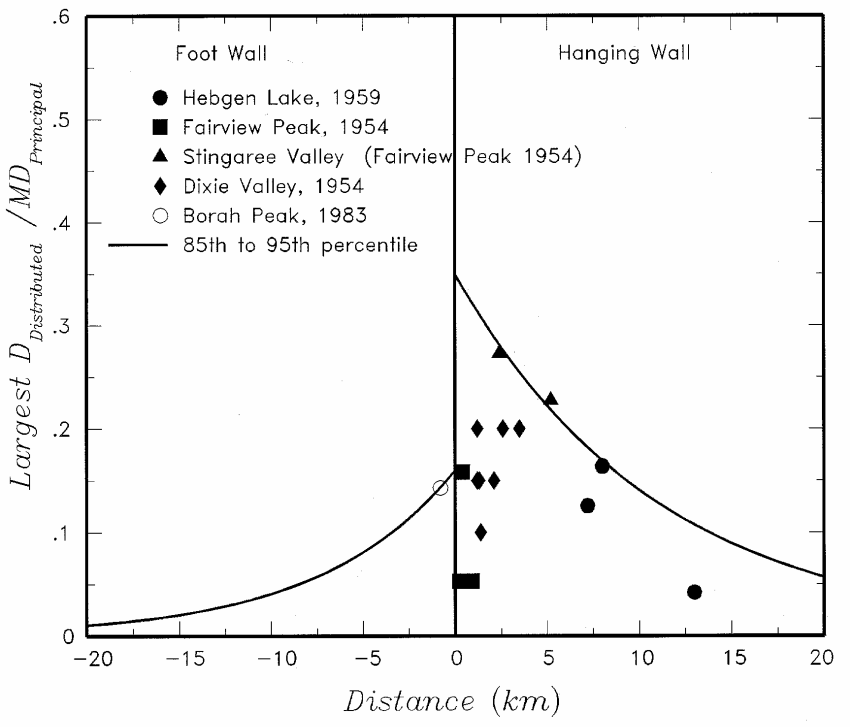

Figure 11. Data for larger displacements on distributed ruptures divided by the maximum displacement on the principal rupture. The curves represent a high percentile (e.g., 85th to 95th) of the distribution for $D_{distributed}$ /$MD_{principal}$. The data were compiled by C. dePolo for the Yucca Mountain PSHA.

DISPLACEMENT APPROACH FOR PFDHA

The relationships for the rate of exceeding a specified level of displacement can be written in simplified form as:

$$n(d) = l_{DE} \cdot P(D > d | \text{Slip}) \tag{10}$$

where l_{DE} is the rate of displacement events and $P(D>d \mid \text{Slip})$ is the conditional probability that the displacement in a single event will exceed value d, given that slip on the feature occurs. In Equation 10 the rate of displacement events on the feature is directly specified without identifying the causal mechanism of these events. Because the source is not treated explicitly, the principal and distributed rupture distinctions are not needed and the conditional probability function $P(\text{slip} \mid \text{event})$ is subsumed into the specification of l_{DE}. Ideally, l_{DE} would be estimated from the age dates for ruptures of a fault and $P(D>d \mid \text{Slip})$ would be estimated from the distribution of measured slip for these ruptures. However, these data are often not available and other approaches are needed to assess l_{DE} and $P(D>d \mid \text{Slip})$. These approaches are described below.

RATE OF DISPLACEMENT EVENTS

There are two techniques for estimation of l_{DE}: direct estimation of recurrence intervals (the inverse of l_{DE}) from paleo-earthquake age data and slip rate data. Where discrete slip events on a fault can be dated, or if the number of events that have occurred within a known time interval can be identified, then the rate of displacement events can be directly assessed. This is the same

approach used to assess the rate of large earthquakes on a fault from paleoseismic data. Where these data are not available, one usually can estimate fault slip rate, *SR*, by dividing the amount of offset for a marker horizon of a known age by the elapsed time. This latter method assumes that the rate of displacement events has been uniform over the elapsed time since the creation of the marker horizon.

When the slip rate and the average slip in a faulting event, $\bar{D}_E$, are known, then l_{DE} can be estimated by:

$$l_{DE} = SR / \bar{D}_E \tag{11}$$

The use of Equation 11 requires an estimate of the average displacement per event, $\bar{D}_E$. For some features (typically those that may be locations of principal faulting), this may be assessed directly from measured offsets exposed by trenching. For other features, scaling relationships that relate $\bar{D}_E$ to a characteristic of the feature of interest, such as total length or cumulative displacement can be used.

Data summarized by Abercrombie (1995, her Figure 11), among others, provide an empirical basis for relating seismic moment to the cube of source dimension (without any assumption about stress drop) over the range in source dimension from 10 m to at least 10 km. The source dimensions are assessed primarily from evaluation of corner frequencies from shear-wave spectra in terms of the radius, *r*, of an equivalent circular fault. Based on the seismic moment equation, these data imply that the average displacement on the fault plane, $\overline{U}$, scales linearly with *r*. In a similar fashion, $\overline{U}$ can be inferred to scale linearly with rupture length, L_R, for roughly equi-dimensional fault ruptures in this range of source dimensions, leading to a scaling relationship of the form:

$$\overline{U} = aL_R \tag{12}$$

where a is a constant of proportionality. Cowie and Scholz (1992) also proposed a scaling relationship of the form of Equation 12 and obtain values of a ranging from 1.5×10^{-5} m/m for continental plate boundary earthquakes to 1×10^{-4} m/m for intraplate earthquakes. In addition, the moment magnitude relationship of Hanks and Kanamori (1979) together with the empirical observation that moment magnitude scales nearly directly with the log of fault area (Wyss 1979, Wells and Coppersmith 1994) leads to Equation 12. In order to use Equation 12, we make the assumption that the rupture length, L_R is equal to the total length of the fault in question, L_{Total}, which allows one to use the mapped length of a feature to estimate $\overline{U}$. We also need to assess the relationship between the average displacement at the surface, $\bar{D}_E$, and the average displacement on the fault plane, $\overline{U}$. Wells and Coppersmith (1994) present data for the ratio $\overline{U}/AD$, where *AD* is again the average displacement at the surface, with a modal value of 1.32. If we assume that $\bar{D}_E$ is equivalent to *AD*, then we obtain the scaling relationship:

$$\overline{D}_E = a' L_{Total} \tag{13}$$

The value of a' derived from the assessments of Cowie and Scholz (1992) ranges from 1.2×10^{-5} to 7.7×10^{-5}. We obtained a value of 3.7×10^{-5} for faults in the Yucca Mountain area from estimates of $\overline{U}$ and L_{Total} for 19 faults (CRWMS M&O 1998).

Another approach to developing a scaling relationship is to relate $\bar{D}_E$ to the cumulative offset on the feature, D_{cum}. Cowie and Scholz (1992) also present relationships between D_{cum} and L_{Total} of the form

$$D_{cum} = ?L_{Total} \quad (14)$$

More recently, rigorous statistical testing by Clark and Cox (1996) of 11 worldwide data sets for faults ranging in length from tenths of a meter to hundreds of kilometers confirm a relationship of the form of Equation 14, with the value of g dependent on the data set analyzed. These data also indicate that g tends to decrease with decreasing fault length. Using Equations 13 and 14 and the arguments presented above, we obtain the scaling relationship:

$$\overline{D}_E = ßD_{cum} \quad (15)$$

For faults in the vicinity of Yucca Mountain, we obtain values for b in the range of 0.0014 to 0.019. Using a similar approach and the data set of Carter and Winter (1995) for faults in the vicinity of Los Alamos, New Mexico, we obtain a b of 0.007.

If both fault slip rate, SR, and the recurrence interval for displacement events, $1/l_{DE}$, can be estimated from the available data, then Equation 11 can be used to estimate $\bar{D}_E$.

CONDITIONAL PROBABILITY OF EXCEEDANCE

The conditional probability of exceedance, $P(D>d \mid \text{Slip})$, specifies the probability that the displacement in a slip event at site k exceeds a specified amount d. The ideal data set to evaluate this distribution is a set of repeated slip events at a single location. Trenching data collected as part of the studies for the Yucca Mountain project provide measurements of multiple displacements at 19 locations. For each trenching site we computed the average displacement per event, $\bar{D}_E$, for paleo-earthquakes, normalized the data at each site by the site average, and then pooled the data. We then tested several distribution forms and found that a gamma distribution provided the best fit to the pooled $D/\bar{D}_E$ data.

Several other normalizing factors were also examined. These include the average displacement for each fault estimated from paleoseismic data from the entire fault, AD_{paleo}; the average displacement for each fault estimated from the fault length and the Wells and Coppersmith (1994) empirical relationship between fault length and average displacement, $AD_{W\&C}$; and the cumulative fault displacement, D_{cum}. Figure 12 shows the resulting pooled data sets and fitted distribution for $D/\bar{D}_E$, D/AD_{paleo}, $D/AD_{W\&C}$, and D/D_{cum}. The parameters of these distributions are listed in the Appendix. Each of these can be used to assess $P(D>d \mid \text{Slip})$, with the appropriate estimate of the normalizing parameter ($\bar{D}_E$, AD_{paleo}, $AD_{W\&C}$, or D_{cum}).

The distributions shown on Figure 12 could also be used to assess the conditional probability of exceedance on a distributed rupture in the earthquake approach with the appropriate normalizing parameter estimated from the characteristics of the fault at the site of interest.

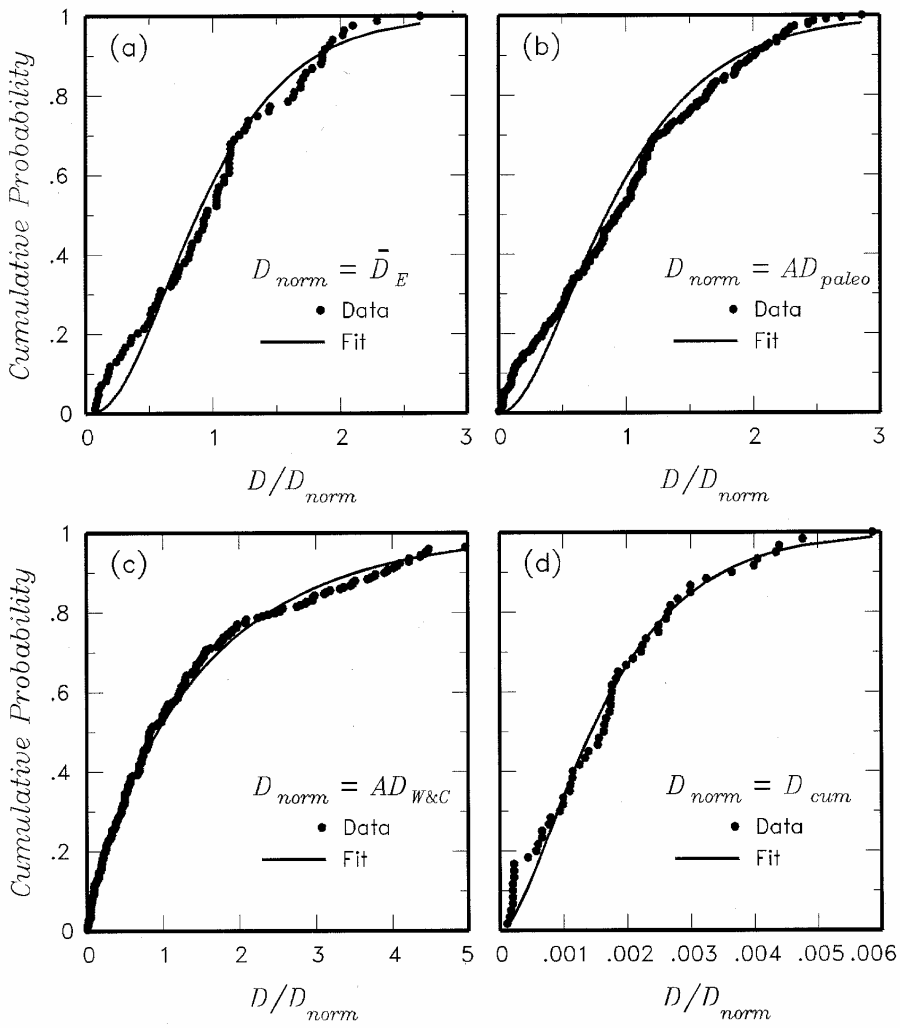

Figure 12. Normalized distributions for displacement per event. The normalizing parameters are: (a) $\bar{D}_E$, the average displacement observed at a site of multiple displacements; (b) AD_{paleo}, the average displacement for a fault estimated from the paleoseismic data for the fault; (c) $AD_{W\&C}$, the average displacement for a fault estimated from fault length and an empirical relationship between length and average displacement; and (d) D_{cum}, the cumulative fault offset.

DISCUSSION

We have presented a framework for conducting a probabilistic assessment of fault displacement hazard at a specific site that is analogous to a probabilistic assessment of ground shaking hazard. This framework is a straight forward extension of the probabilistic methodology for ground shaking hazard with the ground shaking effects conditional probabilistic model [$P(Z>z \mid m,r)$ in Equation 1] is replaced by probabilistic models for the amount of fault offset given the occurrence of an earthquake [$P^*(D>d \mid m,r)$ in Equation 2]. In effect, ground motion attenuation relationships are replaced by "fault displacement attenuation" relationships. These fault displacement attenuation relationships are in an early state of development as evidenced by the wide variety of approaches and probabilistic models that we have proposed. The immaturity of these models leads to greater uncertainty in the computed fault displacement hazard than one would obtain for a ground motion assessment in the same tectonic environment, as indicated in the applications of this methodology (CRWMS M&O

1998, Olig et al. 1998, Braun 2000, Stepp et al. 2001). Consequently, it is important that a formal treatment of uncertainty be incorporated into the application of the methodology. Uncertainty in hazard characterization is now a standard part of PSHA studies (see NRC 1988, SSHAC 1997) and the methodologies are directly transferable to PFDHA.

A formal treatment of uncertainty was used in the application of the methodology described in this paper to the assessment of fault displacement hazard at Yucca Mountain, Nevada (CRWMS M&O 1998, Stepp et al. 2001) and Los Alamos, New Mexico (Olig et al. 1998) and the relative weighting of the models presented in this paper is documented in those studies. Figure 13 shows the general form of the logic tree used in those studies to assess uncertainty in the PFDHA for principal faulting. The first node addressed the use of the two alternative approaches. Following the earthquake approach branch, there are four nodes that represent the uncertainty in characterizing the seismic source. These nodes would be identical to those developed for a ground-shaking hazard PSHA. The next two nodes on the earthquake approach branch address relative weighting of the alternative approaches for assessing the conditional probability of slip, $P_{kn}(\text{Slip} \mid m,r)$. The last two nodes address weighting alternative approaches for assessing the conditional distributions for fault slip at a point, given an earthquake surface rupture. The lower level of the logic tree outlines the uncertainty treatment for the displacement approach. The first two nodes address the uncertainty in the displacement event recurrence and the last two nodes address uncertainty in characterizing the average displacement and the conditional distribution for displacement in a single event.

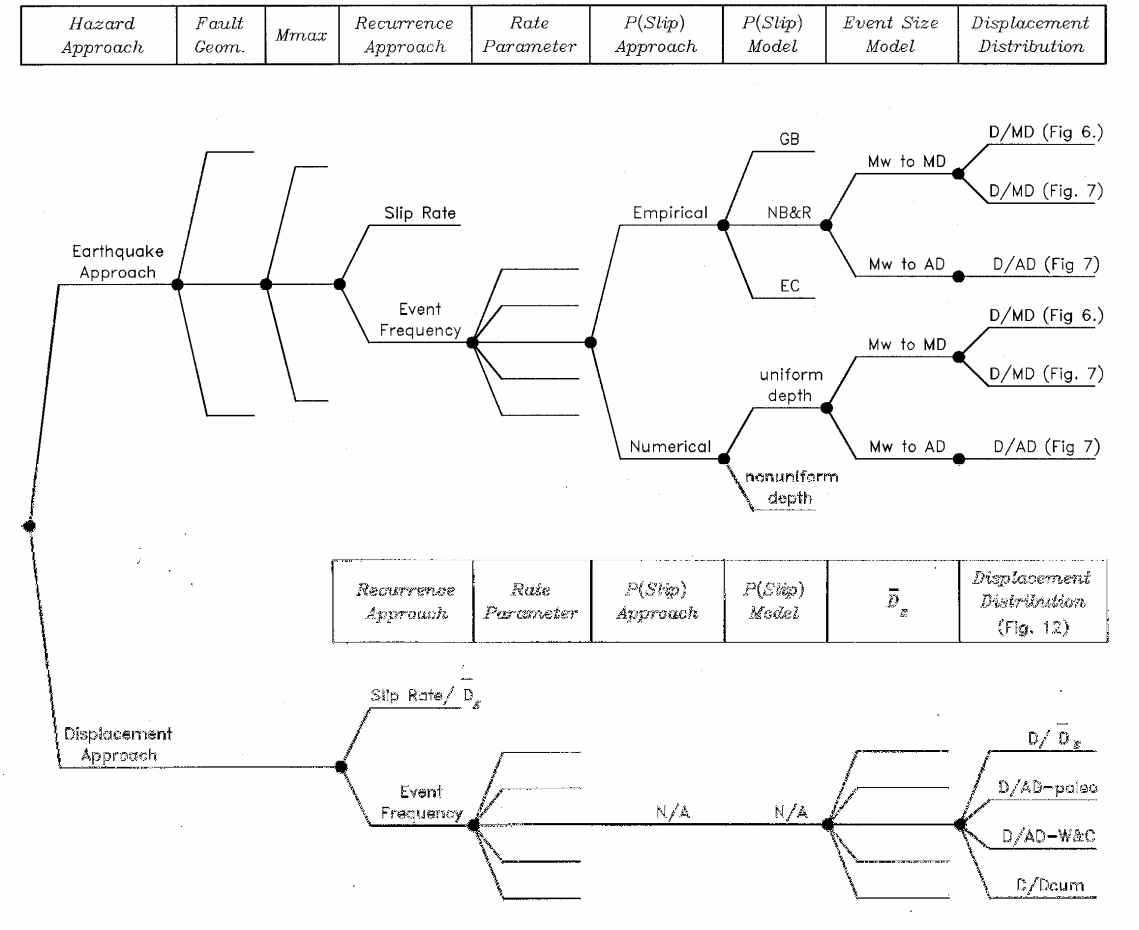

Figure 13. Generalized logic tree for PFDHA.

Figure 14 shows example PFDHA results from the Yucca Mountain and Los Alamos studies. Each plot shows the mean hazard curve and hazard curves corresponding to the 15th, 50th, and 85th percentiles of the distribution for rate of exceedance. The uncertainty in rate of exceedance is large at large displacement levels. The large uncertainty arises because of the limited data sets that are available for characterizing the various probability distributions, particularly for distributed faulting hazard. The distributions described above and listed in the Appendix were derived primarily for normal faulting earthquakes and, in some cases are focused on faulting in a limited region (e.g., faulting within Yucca Mountain, Nevada). Improvement in the models for surface faulting in this environment will require compilation of the appropriate data that describe the detained characteristics of faulting, particularly distributed faulting. These improvements can come principally from detailed mapping of earthquake rupture patterns and fault offsets, providing the opportunity to develop better-constrained probability models.

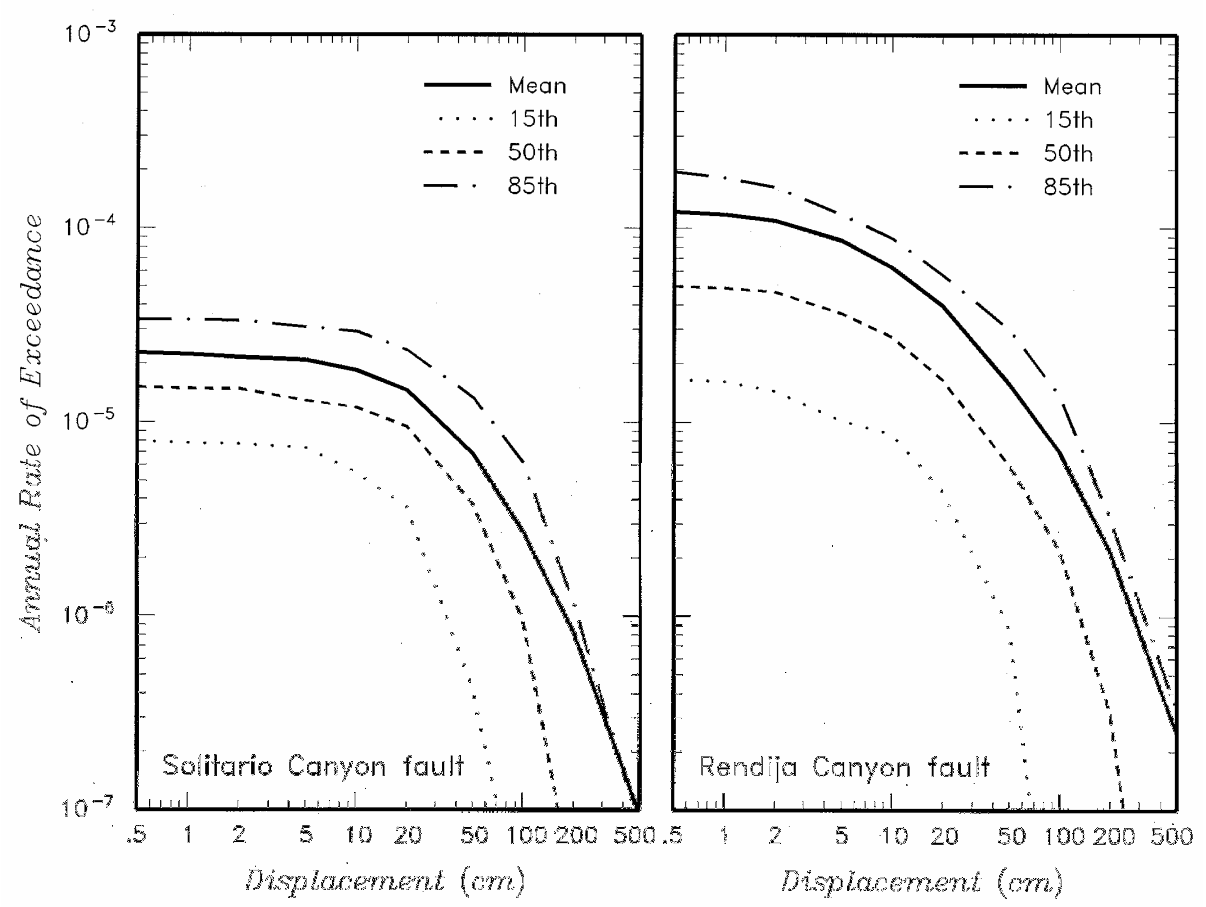

Figure 14. Example displacement hazard curves resulting from PFDHA calculations for sites on the Solitario Canyon fault at Yucca Mountain, Nevada and on a possible extension of the Rendija Canyon fault at Los Alamos, New Mexico. Shown are the mean hazard curves and hazard curves corresponding to the 15th, 50th, and 85th percentiles of the distribution for rate of exceedance.

The general methodology is applicable to all types of tectonic environments. What are needed to perform PFDHA in regions of strike-slip or reverse faulting are fault displacement attenuation relationships for these types of earthquakes. In particular, compilations and analysis of data for slip distributions along the principal fault rupture (similar to the data shown of Figure 5 for normal faulting earthquakes) and analysis of mapped distributions of distributed

faulting (similar to the data shown on Figure 3) would be needed to develop these relationships for other types of faulting.

In closing, we point out some characteristics of the result of a PFDHA calculation. The example hazard curves shown on Figure 14 represent the relationship between the amount of displacement in a *single* event and the rate of events that produce larger displacements in the same way that a ground motion hazard curve represents the relationship between the level of shaking and the rate at which it is exceeded. The first thing to notice is that the displacement hazard curves have a somewhat different shape than typical ground motion hazard curves (see part 4 of Figure 1) in that the rate of exceedance does not continue to increase as the displacement amplitude decreases. The reason for this difference in shape at low amplitudes is due to the introduction of the conditional probability of slip term, $P_{kn}(\text{Slip} \mid m,r)$, into the formulation of Equation 3. As discussed above, whereas every earthquake is expected to produce some level of shaking at a site, not every earthquake is expected to produce slip on a feature. Thus all of the small and/or distant earthquakes that contribute to the hazard at low levels of ground shaking do not produce low levels of slip on the feature of interest. For the displacement approach, the term $P_{kn}(\text{Slip} \mid m,r)$ is implicitly incorporated into the calculation of the rate of slip events, l_{DE}. From Equation 10 one can see that the rate of exceedance, $n_k(d)$, can never be greater than the rate of slip events and the shape of the hazard curve for the displacement approach is defined by the complementary cumulative distribution function for the displacement per event.

The second point of interest is that an effective slip rate can be derived from the displacement hazard curve, allowing a check of the results. The negative of the slope of the hazard curve, $-\mathrm{d}n_k(d)/\mathrm{d}d$, is the rate density of displacements of amount d. Assuming that all displacement events produce slip in the same direction, integrating the product of the rate density, $-\mathrm{d}n_k(d)/\mathrm{d}d$, and the amount of displacement, d, provides an estimate of fault slip rate, SR. Specifically:

$$SR_k = \int_0^\infty \left[-\mathrm{d}n_k(d)/\mathrm{d}d \times d \right] \mathrm{d}d \tag{16}$$

Using integration by parts, the above integral may be expressed directly in terms of the hazard curve, obtaining:

$$SR_k = \int_0^\infty n_k(d)\,\mathrm{d}d \tag{17}$$

The resulting effective slip rate can be compared with direct estimates for the feature to provide a check on the reasonableness of the computed hazard. For example, application of Equation 17 to the hazard curves for the mean hazard curves shown on Figure 14 yields slip rates of 0.001 and 0.003 cm/yr (0.01 and 0.03 mm/yr), respectively. These values are consistent with the typical range of directly assessed slip rates of 0.005 to 0.02 mm/yr for the Solitario Canyon fault (CRWMS M&O 1998) and 0.01 to 0.06 mm/yr for the Rendija Canyon fault (Olig et al. 1998).

ACKNOWLEDGMENTS

The work presented in this paper was developed as part of assessments of seismic hazards at Yucca Mountain, Nevada, and the Los Alamos National Laboratory, New Mexico. The work for Yucca Mountain was performed under the auspices of the U.S. Geological Survey with

support from the CRWMS M&O Contractor TRW Environmental Safety Systems, Inc. and DOE under contract DE-AC04-94AL85000. The work for Los Alamos was performed for the Los Alamos National Laboratory and the University of California under contract 5212F0016-CE-118. We also wish to acknowledge the helpful comments of three anonymous reviewers.

APPENDIX -PROBABILITY DISTRIBUTIONS FOR PFDHA

Listed in this appendix are the specific probability models illustrated in the text of the paper. Conceptually, these can be considered as alternative fault displacement attenuation functions. It is recommended that application of the PFDHA methodology incorporate an explicit treatment of uncertainty. Within such an uncertainty treatment, multiple probability models for fault displacement should be used with weights assigned based on their applicability to the site under study.

Coefficients for Equation 4 shown on Figure 4

Data Set	*a*	*b*
Data from Pezzopane and Dawson (1996)		
32 Great Basin earthquakes	-16.02	2.685
47 northern Basin & Range earthquakes	-18.71	3.041
105 extensional cordillera earthquakes	-12.53	1.921
Data from Wells and Coppersmith (1993)		
276 world wide earthquakes	-12.51	2.053

Coefficients for beta distribution for *D/MD* shown on Figure 6

$$a = \exp[0.6064+21.83x/L -108.0(x/L)^2 +136.6(x/L)^3]$$
$$b = \exp[2.027+12.21x/L -87.90(x/L)^2 +115.5(x/L)^3]$$
$$\text{with } 0 \le x/L \le 0.5$$

Coefficients for beta distribution for *D/MD* shown on Figure 7

$$a = \exp(-0.705+1.138x/L)$$
$$b = \exp(0.421-0.257x/L).$$
$$\text{with } 0 \le x/L \le 0.5$$

Coefficients for gamma distribution for *D/AD* shown on Figure 7

$$a = \exp(-0.193+1.628x/L)$$
$$b = \exp(0.009-0.476x/L)$$
$$\text{with } 0 \le x/L \le 0.5$$

Coefficients for logistic regression model for probability of slip for distributed rupture

For Equation 7

$$f(x) = 2.06 + (-4.62 + 0.118m + 0.682h) \cdot \ln(r + 3.32)$$

The goodness of fit statistic $\hat{C}$ = 317 with a *p*-value of 0.00.

For Equation 8

$$f(x) = 3.27 + (-8.28 + 0.577m + 0.629h) \cdot \ln(r + 4.14) + 0.611z_i$$

The goodness of fit statistic $\hat{C} = 8.4$ with a *p*-value of 0.68.

Coefficients of Equation 9

Data Set	C_1	C_2	C_3
n ≥ 2	-2.09	-0.0732	-0.00546
n ≥ 3	-1.84	-0.130	-0.00415
n ≥ 4	-1.73	-0.173	-0.00226
n ≥ 5	-1.72	-0.186	-0.00132
n ≥ 6	-1.86	-0.0734	-0.0117

Coefficients for 85th to 95th percentile of distribution for $D_{distributed}/MD_{principal}$ shown on Figure 11.

$$D_{distributed}(\text{hanging wall})/MD_{principal} = 0.35 \times \exp(-0.091r)$$
$$D_{distributed}(\text{footwall})/MD_{principal} = 0.16 \times \exp(-0.137r)$$

Coefficients of gamma distributions for D_{norm} shown on Figure 12.

D_{norm}	*a*	*B*
$\bar{D}_E$	2.71	0.369
AD_{paleo}	2.17	0.461
$AD_{W\&C}$	0.821	1.77
D_{cum}	1.79	0.000983

REFERENCES CITED

Abercrombie, R. E., 1995, Earthquake source scaling relationships from –1 to 5 M_L using seismograms recorded at 2.5-km depth, *Journal of Geophysical Research*, **100** 24,015-24-036.

Braun, J., 2000, *Earthquake Displacement Hazard of the Wasatch and Surrounding Faults, Wasatch Front, Utah*, M.S. Thesis, Department of Geology and Geophysics, University of Utah, Salt Lake City, UT., 111 pp.

Brillinger, D. R., and Preisler, H. K., 1983, Maximum likelihood estimation in a latent variable problem: in *Studies in Econometrics, Time Series, and Multivariate Statistics*, S. Karlin, T. Amemiya, and L. A. Goodman (eds.), Academic Press, New York, 31-65.

Carter, K. E., and Winter, C. L., 1995, Fractile nature and scaling of normal faults in the Española Basin, Rio Grande Rift, New Mexico: Implications for fault growth and brittle strain, *Journal of Structural Geology*, **17**, 863-873.

Civilian Radioactive Waste Management System Management and Operating Contractor (CRWMS M&O), 1998, Probabilistic seismic hazard analyses for fault displacement and vibratory ground motion at Yucca Mountain, Nevada, *U.S. Department of Energy DE-AC04-94AL85000*, Prepared for the U.S. Geological Survey, February 23, 3 vols.

Clark, R. M., and Cox, S. J. D., 1996, A modern regression approach to determining fault displacement-length scaling relationships, *Journal of Structural Geology*, **18**, (2/3), 147-152.

Coppersmith, K. J., and Youngs, R. R, 1992, Modeling fault rupture hazard for the proposed repository at Yucca Mountain, Nevada, *Proceedings of the Third International Conference on High Level Radioactive Waste Management*, Las Vegas, Nevada, April 12-16, **1**, 1142-1150.

Cornell, C. A., 1968, Engineering seismic risk analysis, *Bulletin of the Seismological Society of America*, **58**, 1583-1606.

Cornell, C. A., 1971, Probabilistic analysis of damage to structures under seismic loads, in *Dynamic Waves in Civil Engineering*, Howells, D. A., Haigh, I. P., and Taylor, C. (eds.), John Wiley, London.

Cowie, P. A., and Scholz, C. H., 1992, Growth of faults by accumulation of seismic slip, *Journal of Geophysical Research*, **97**, 11,085-11,096.

dePolo, C. M., 1994, The maximum background earthquake in the basin and range, *Bulletin of the Seismological Society of America*, **84**, 466-472.

Hanks, T.C., and Kanamori, H., 1979, A moment-magnitude scale, *Journal of Geophysical Research*, **84**, 2348-2350.

Hemphill-Haley, M. A. and Weldon, R. J. II, 1999, Estimating prehistoric earthquake magnitude from point measurements of surface rupture, *Bulletin of the Seismological Society of America*, **89**, 1264-1279.

Hosmer, D. I. and Lemeshow, S., 1989, *Applied Logistic Regression*, John Wiley & Sons, New York, 307 pp.

McCalpin, J. P. and Slemmons, D. B., 1998, Statistics of paleoseismic data, Unpublished final technical report submitted to the U.S. Geological Survey by GEO-HAZ Consulting, Inc., 62 pp.

McGuire, R. K., Bullen, D. B., Cook, N., Coppersmith, K. J., Long, A., Pearson, F. J., Schwartz, F., Sheridan, M., and Youngs R. R., 1990, *Demonstration of a Risk-Based Approach to High-Level Waste Repository Evaluation*, *Report NP-7057* prepared for the Electric Power Research Institute, Research Project 3055-2, October.

National Research Council, 1988, *Probabilistic Seismic Hazard Analysis*, National Academy Press, Washington, DC., 97 pp.

Olig, S., Youngs, R., and Wong, I., 1998, *Probabilistic seismic hazard analysis for surface fault displacement at TA-3, Los Alamos National Laboratory*, report prepared for Los Alamos National Laboratory, University of California, July.

Pezzopane, S. K. and Dawson, T. E., 1996, Fault displacement hazard: A summary of issues and information, in *Seismotectonic Framework and Characterization of Faulting at Yucca Mountain, Nevada*, U.S. Geological Survey Administrative Report prepared for the U.S. Department of Energy, Chapter 9, 160 pp.

Power, M. S., Perman, R., Wesling, J., Youngs, R. R, and Shimamoto, M., 1991, Assessment of liquefaction potential in the San Jose, California urban area, *Proceedings of the 4th International Conference on Seismic Micro-Zonation*, Stanford, California, **II**, 677-625.

Senior Seismic Hazard Analysis Committee (SSHAC), 1997, *Recommendations for Probabilistic Seismic Hazard Analysis – Guidance on Uncertainty and Use of Experts*, U.S. Nuclear Regulatory Commission (NRC), *NUREG/CR-6372*, Washington, DC.

Stepp, J. C., Wong, I., Whitney, J., Quittmeyer, R., Abrahamson, N., Toro, G., Youngs, R., Coppersmith, K., Savy, J., Sullivan, T., and Yucca Mountain PSHA Project Members, 2001, Probabilistic seismic hazard analyses for fault displacement and ground motions at Yucca Mountain, Nevada, *Earthquake Spectra*, **17** (1), 113-151.

U.S. Department of Energy (USDOE), 1997, *Topical Report YMP/TR-002-NP-Methodology to Assess Fault Displacement and Vibratory Ground Motion Hazards at Yucca Mountain*, Revision 1: Civilian Radioactive Waste Management System Management and Operating Contractor.

Wells, D. L. and Coppersmith, K. J., 1993, Likelihood of surface rupture as a function of magnitude (abs.), *Seismological Research Letters*, **64** (1), 54.

Wells, D. L., and Coppersmith, K. J., 1994, New empirical relationships among magnitude, rupture length, rupture width, rupture area, and surface displacement, *Bulletin of the Seismological Society of America*, **84**, 974-1002.

Wheeler, R. L., 1989, Persistent segment boundaries on basin-range normal faults, in *Proceedings, Conference XLV-Fault Segmentation and Controls on Rupture Initiation and Termination*, eds. D. P. Schwartz and R. H. Sibson, *U.S. Geological Survey Open-File Report 89-315*, 432-444.

Wyss, M., 1979, Estimating maximum expected magnitude of earthquakes from fault dimensions, *Geology*, **7**, 336-340.